

Phenol Removal using Corona Discharge Plasma Combined with Porous Polyaniline Nanofiber

Ahmed El-Tayeb Khalil (✉ Ahmed_al_tayeb@aswu.edu.eg)

Aswan University <https://orcid.org/0000-0001-8719-8715>

Hussain Noby

Egypt-Japan University of Science and Technology

AHMED H ELSHAZLY

Egypt-Japan University of Science and Technology

Marwa F. Elkady

Egypt-Japan University of Science and Technology

Research Article

Keywords: Non-Thermal Plasma, Corona Discharge Plasma, Industrial Water Treatment, Organic Pollution, Polyaniline Nanofiber, Phenol Removal

Posted Date: May 11th, 2021

DOI: <https://doi.org/10.21203/rs.3.rs-441230/v1>

License: © ⓘ This work is licensed under a Creative Commons Attribution 4.0 International License.

[Read Full License](#)

Phenol Removal using Corona Discharge Plasma Combined with Porous Polyaniline Nanofiber

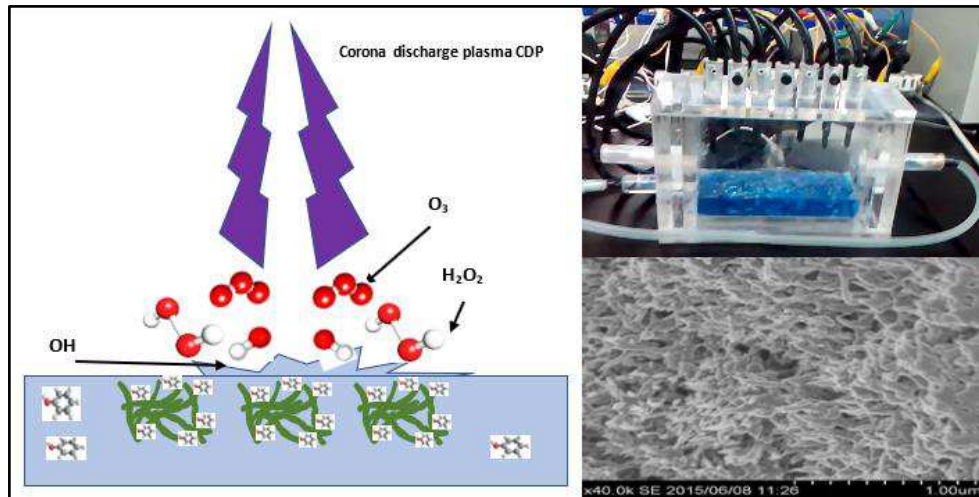
Ahmed EL-Tayeb Khalil ^{1,*}, Hussain Noby^{2,3}, Ahmed Hassan EL-Shazly ³, Marwa Elkady³

¹ Electrical Engineering Department, Faculty of Energy Engineering, Aswan University, Aswan, Egypt.

² Materials Engineering and Design Department, Faculty of Energy Engineering, Aswan University, Aswan, Egypt.

³ Chemical and Petrochemicals Engineering Department, Egypt-Japan University of Science and Technology, New Borg El-Arab City, Alexandria, Egypt.

*Corresponding author: Ahmed_Al_Tayeb@aswu.edu.eg



Abstract

A contemporary design for a recirculated flow dual remediation system was successfully developed for phenol remediation. The system involved Corona Discharge Plasma (CDP), accompanied by Polyaniline Nanofiber (PANNFs) as a solid adsorbent. PANNFs was obtained using simple chemical oxidation polymerization at room temperature. Different chemo-physical characterization techniques were employed to examine the produced polyaniline such as Fourier Transform Infrared spectroscopy (FT-IR), X-ray Diffraction (XRD), and Brunauer, Emmett, and Teller (BET) surface area analysis. The primary purpose of the used PANNF powder is to facilitate the phenol degradation using plasma by collecting the phenol molecules on the surface of PANNFs. The phenol removal percentage of 99% was attained at a treatment time of 60 min using the developed dual system. Finally, a slight synergetic effect between the used two remediation processes, PANI as adsorbent and CDP treatment, was approved. PANNFs existence in the remediation system also helps to save the consumed power in degradation using CDP.

Keywords: Non-Thermal Plasma; Corona Discharge Plasma; Industrial Water Treatment; Organic Pollution; Polyaniline Nanofiber; Phenol Removal.

1 Introduction

Phenol and its derivatives are vastly used in various industries such as fertilizers, plastics, paints, paper and soap industries, adhesives petroleum refineries, coal gasification processes, liquefaction

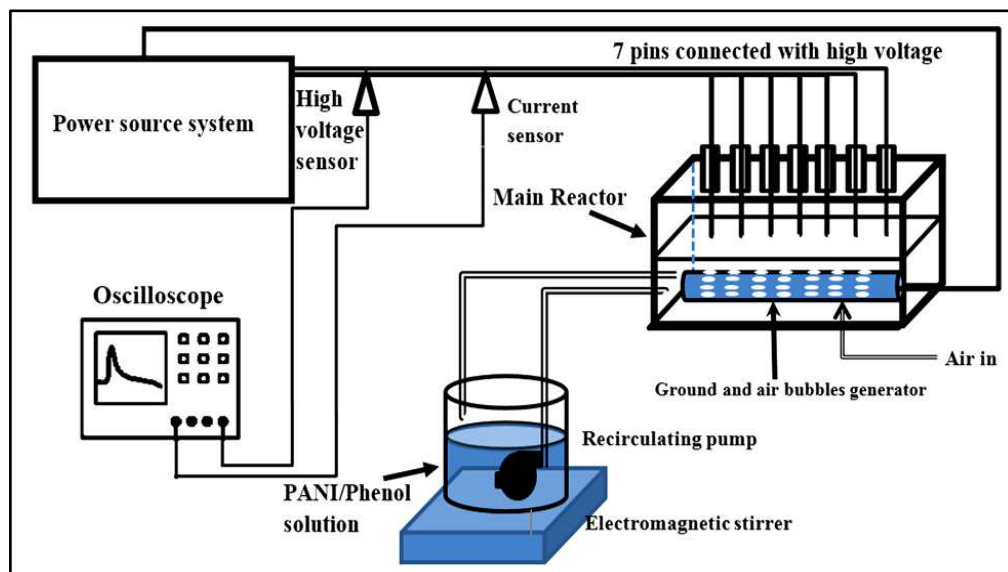
30 processes, and phenol-formaldehyde resins (Bakelite). Although the concentrations of phenol are a
31 vital issue of environmental concern due to their toxicity (Seo et al. 2013, Kulkarni et al. 2013), no
32 more than 5 mg/L phenol concentration is allowed conferring to the Environmental Protection
33 Agency (EPA) regulations (Belaib et al. 2012). For instance, erosion of tissues, protein degeneration,
34 paralysis of the central nervous system, and damages of kidneys, liver, pancreas are kinds of
35 infections that could occur if a phenol contaminated water were consumed by a human body (Belaib
36 et al. 2012, Bosi et al. 2018 and Ni et al. 2013). Therefore, regarding preserving the environmental
37 and health quality, phenol removal from aqueous solutions is a crucial concern. Numerous techniques,
38 such as solvent extraction, dialysis, microbial degradation, ion exchange, reverse osmosis, membrane
39 processes, non-thermal plasma, and adsorption, were investigated for phenol removal from
40 wastewater (Jiang et al. 2014, El-Tayeb 2016). Among the mentioned techniques, non-thermal
41 plasma was highly considered due to its high selectivity and energy efficiency in chemical reactions
42 compared with the thermal plasma, which needs high energy. Therefore, electrical plasma
43 technologies for water treatment attracted an increasing interest. Significant bulk-phase reactions
44 could be generated on the surface of the liquid by the plasma. These reactions generated at the air-
45 liquid interface resulted in oxidative reagents generation. The generated reagents, such as: OH^* , O^* ,
46 O_2 , and H^* and different molecules like H_2O_2 and O_3 , were used successfully for water
47 decontamination (El-Tayeb et al. 2016, An et al. 2011). Coalescence of two forms of advanced
48 removal techniques is a promising approach in wastewater treatment processes. The pulsed discharge
49 plasma system with TiO_2 photo-catalysis was combined for target pollutants oxidization in aqueous
50 solution (Zhang et al. 2013, Iervolino et al. 2019). Also, pulsed discharge plasma with activated
51 carbon was employed for wastewater purification and treatment (Hao et al. 2009, Jiang et al. 2013).
52 Polyaniline (PANI) is an active conductive polymer with unique properties such as chemical stability,
53 considerable surface area, ease in preparation, and non-toxic. Consequently, PANI was widely used
54 in wastewater treatment (El-Tayeb et al. 2016, El-Tayeb et al. 2017, Xu et al. 2015). Accordingly, it
55 was inspired to study the effect of non-thermal plasma degradation with PANI adsorption
56 combination. Herein, a dual remediation system was introduced for phenol removal from aqueous
57 solutions. The phenol solution is treated by polyaniline nanofibers (PANNFs) adsorbent before being
58 degraded by plasma. This system examines the combination of the adsorptive removal using PANNFs
59 with the phenol degradation using the non-thermal plasma system. The phenol degradation process
60 was optimized experimentally by studying the change of the phenol initial concentration and the
61 dosage of the PANNFs.

62

63 **2 Material and Method**

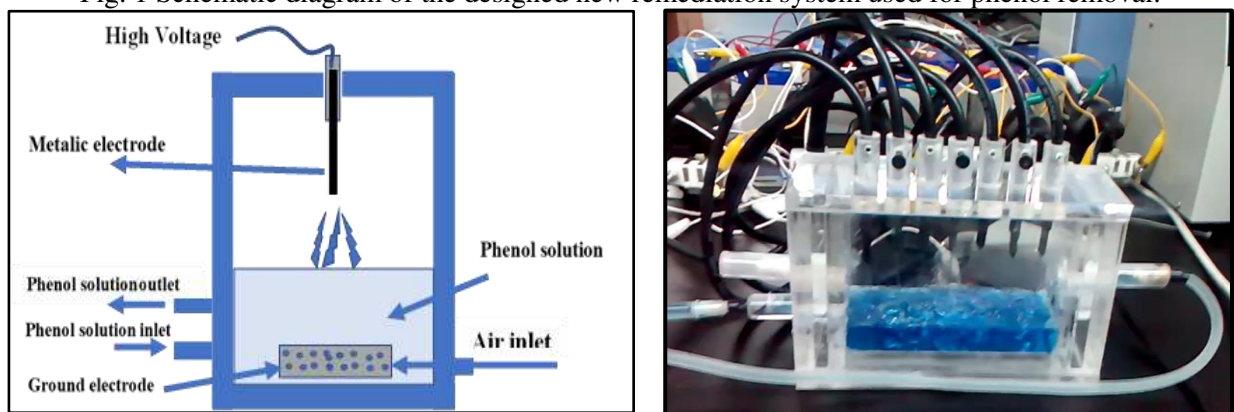
64 **2.1 Corona Discharge Plasma System**

65 The experimental setup is shown in Fig. 1 is composed of two main parts, the electrical power supply
 66 system, and non-thermal plasma-based reactor. First, the electrical power supply system consists of
 67 three parts; DC battery, Pulsed Wide Modulation (PWM) switching circuit, and an ignition coil
 68 (autotransformer). The DC battery is responsible for providing a DC voltage of 12 V to an electronic
 69 switching circuit PWM. The output of the PWM circuit is a pulsed voltage directed to the ignition
 70 coil, which in turn converts the low voltage to a high voltage of 15 KV. Voltage and current sensors
 71 are placed after the ignition coil and connected to an oscilloscope to show the waveforms of the
 72 voltage and current. High voltage generated is applied to the electrodes to produce the electrical
 73 discharge between the high voltage electrode and the ground one which called Corona Discharge
 74 Plasma as a type of Non-thermal Plasma technique for industrial wastewater treatment.



75
76

Fig. 1 Schematic diagram of the designed new remediation system used for phenol removal.



77
78

Fig. 2 Schematic diagram of the main reactor's side view.

79 Second, the reactor consists of a high voltage pin electrode (7 pins) fixed over a rectangle vessel (21
 80 *7*10 cm), tube as a ground electrode, recirculating water pump, and circular reservoir placed over
 81 a stirrer. The pins electrodes were fixed vertically 15 mm over the wastewater surface. The seven pins
 82 have 1 mm in diameter, 30 mm in height, placed in a linear pattern 15 mm apart of each other's, and

83 connected to the high voltage cables. The ground stainless-steel tube was submerged in the liquid and
84 perforated to be used as an air inlet for wastewater agitation. At the reservoir, the contaminated water
85 (aqueous phenol solution) was mixed with PANI powder, stirred at 500 rpm for a certain time, and
86 then recirculated through the system at 150 mL/min using a submerged water pump (without
87 preventing water stirring). Air was pumped into the ground electrode tube using a compressor with a
88 uniform flow rate of 0.1 L/min. The air passed from the tube to the discharge region across the
89 wastewater vessel. Then, the air and the gases resulted from the phenol degradation passed the pipe
90 between the discharge region and the reservoir, before being released from the reservoir.

91 **2.2 Polyaniline preparation**

92 **2.2.1 Materials**

93 Aniline $C_6H_5NH_2$, ammonium peroxydisulfate (APS) $(NH_4)_2S_2O_8$, HCl, ethanol, methanol, and
94 Phenol (Sigma Aldrich, USA) were used as received.

95 **2.2.2 Polyaniline synthesis**

96 A simple chemical polymerization process with a rapid mixing technique was used to produce the
97 nanofiber polyaniline (PANNFs). 0.2 M aniline was dissolved in 50 mL of 1 M HCl solution at room
98 temperature. Another 50 mL aqueous solution of 0.25 M APS was also prepared at room temperature.
99 The APS solution was mixed with the aniline solution at once with continuous stirring at 1000 rpm
100 for 1 hr. The polymerization process was kept for 24 hours at room temperature. The precipitated
101 polymer powder was filtered, collected, and washed with 0.2 M of HCl, ethanol, methanol, and
102 distilled water then separated by centrifugation for 15 min at 5000 rpm. Then, the produced polymer
103 was dried overnight at 60 °C.

104 **2.3 Characterization techniques**

105 The FT-IR spectra and X-ray diffraction analysis of the produced PANI were measured using an IR
106 spectrometer (Vertex 70, Bruker Scientific Instruments, Germany) and LabX XRD-6100 (Shimadzu,
107 Japan), respectively. Scanning Electron Microscopy (SEM, JEOL JSM 6360LA, Japan) was
108 employed to show the produced morphology. Nitrogen adsorption/desorption isotherms at 77 K and
109 Brunauer–Emmett Teller (BET) surface area tests were conducted using a Belsorp Mini II (BEL Japan
110 Inc., Japan). The pore size distribution and the total pore volume were evaluated using the Barrett,
111 Joyner, and Halenda (BJH) method. The classification of pores and isotherms standardized by The
112 International Union of Pure and Applied Chemistry (IUPAC) was used in this study. The phenol
113 concentration before and after the treatment process was measured using a UV spectrometer
114 (HITACHI U-3900).

115 **2.4 Energy Consumption Evaluation**

116 2.4.1 Energy Consumption

117 A significant factor in identifying the feasibility of phenol degradation using the newly designed
118 system is the power consumption estimation for a fixed quantity of wastewater and treatment time.
119 The consumed energy consumed per unit volume (E_c) (J/L) is calculated using Eq. (2).

$$121 E_c = \frac{t * P}{V_o} \quad (2)$$

122 Where t is the treatment time (s), P is the power (W), and V_o is the solution volume (L).

124 2.5.2 Electrical Energy per Order

125 Electrical energy per order (EE/O) is a vital term to estimate the consumed electrical power in the
126 treatment process. EE/O was defined as; the electrical energy in kilowatt-hours (kWh) required to
127 reduce the concentration of a pollutant by 1 order of magnitude in 1 m³ of contaminated water. EE/O
128 (in kWh/m³) is calculated by (Sunka 2001, Wang et al. 2014):

$$129 EE/O = \frac{P * t * 1000}{60 * V_o * \log(C_i/C_f)} \quad (3)$$

130 Where C_f is the final phenol concentration (mg/L).

131 2.5.3 Energy yield for phenol remediation

132 The energy yield (G) (g/kWh) is defined as the amount of pollutant in grams could be decontaminated
133 when 1 kWh of powers is consumed. It could be calculated using the following relation, (Lukes 2005,
134 Hayashi et al. 2014):

$$135 G = \frac{C_o * V_o * D\%}{100 * P * t} \quad (4)$$

136 Where $D\%$ is the percentage of phenol removal, C_o in (mg/L), P in (kW), and t (hour).

138 3 RESULTS AND DISCUSSION

140 PANNFs weight of (0, 0.05, 0.1, 0.15, 0.2, and 0.25 g) were mixed with 400 mL of phenol/water
141 solution with phenol initial concentration of (5, 10, 20, 40, 60, 80, and 100 mg/L). The mixtures were
142 stirred at 500 rpm continuously at room temperature. After a while, the mixture was recirculated by
143 a pump with a flow rate of 150 mL/min to the reactor and then exposed to the Corona Discharge
144 Plasma System (CDPS). The reactor was extra agitated with fresh air pumped into the system with a
145 flow rate of 0.1 L/min. Furthermore, a typical experiment was conducted using 0.25 g of PANNFs
146 alone without plasma to measure the proposed synergy effect between the two phenol removal
147 techniques. 1 mL of the solution was drawn After a time interval of 10 min, and the phenol
148 concentration was measured using a UV spectrophotometer (HITACHI U-3900) at a wavelength of
149 265 nm. The remediation efficiency RE of the dual system was calculated by:

150
$$\% RE = (C_0 - C_t) / C_0 * 100 \tag{1}$$

151
 152 Where C_0 and C_t are the initial phenol concentration [mg/L] and the concentration at time t ,
 153 respectively.

154 **3.1 Polyaniline characterization**

155 **3.1.1 Morphology of PANI**

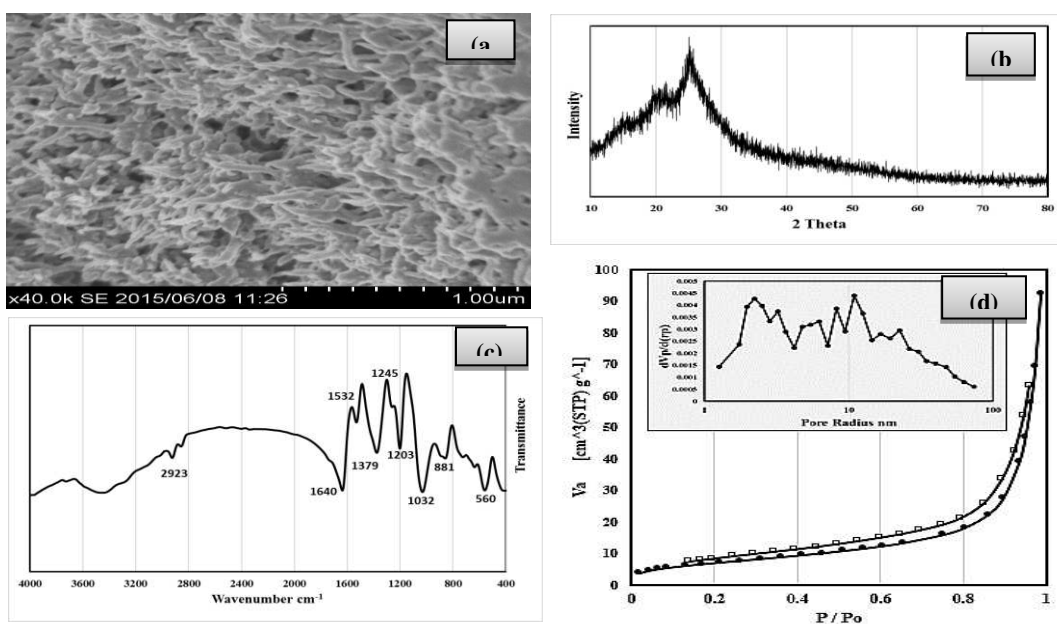
156 The morphology of the prepared PANI was observed by SEM. Figure 3a showed that nanofibers were
 157 obtained with an average diameter of 40 nm. Furthermore, it was noticed that the fibers were directed
 158 in one direction with a rough surface. The rough surface may help increase the surface area which
 159 plays a crucial role in the adsorption process.

160 **3.1.2 Crystalline structure**

161 As shown in Fig. 3b, a classic semi-crystalline structure with a considerable agreement with what
 162 reported before (Ai et al. 2010, Ayad et al. 2013, Noby et al. 2017). The formed crystals may result
 163 from the existence of hydrogen bonds between amines and imines in the longitudinal direction of the
 164 polyaniline chain. The XRD pattern of PANI shows two peaks: one centered at $2\theta=21^\circ$, which could
 165 be ascribed to a periodicity parallel to the PANI polymer chain, and the other at 25.7° could be
 166 ascribed to a periodicity perpendicular to the PANI chain (Noby et al. 2016).

167 **3.1.3 Chemical structure**

168 The Fourier transform infrared spectra (FT-IR) of PANNFs were shown in Fig. 3c. The FT-IR spectra
 169 agree with the previously reported results (Noby et al. 2018, Noby et al. 2019, Kaneko 1994). The
 170 characteristic peaks of the benzenoid and quinoid units at 1532 and 1640 cm^{-1} , respectively, were
 171 identified.



172
 173 Fig. 3 (a) SEM image, (b) XRD, (c) FT-IR, and (d) N_2 adsorption/desorption isotherm and pore size
 174 distribution for the produced PANI.

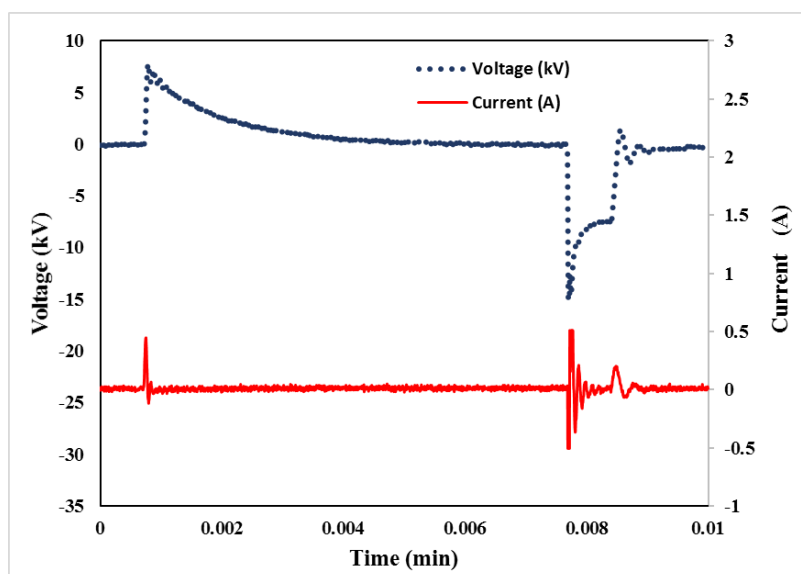
175 The band at 1379 cm^{-1} was attributed to the C—N stretching vibration of the secondary aromatic
176 amine. The peak at 695 cm^{-1} is accompanied by the aromatic C—H out-of-plane bending vibrations.
177 The band at 1203 cm^{-1} corresponds to N=Q=N, where Q represents the quinoid unit. The band at 881
178 cm^{-1} is associated with C—C and C—H for the benzenoid unit.

179 3.1.4 Surface area and pore size of the synthesized PANI

180 BET surface area and average pore size curves of the attained PANNFs are displayed in Fig. 3d. The
181 BET surface area was $26.42\text{ m}^2/\text{g}$ accompanied by hysteresis loop H_3 type, which means that the
182 pores were slit-shaped (Noby et al. 2019, Rather et al. 2015). Additionally, PANI has a wide pore
183 size distribution (diameters from 1.4 to 90 nm), which may be considered as macroporous structures
184 according to the IUPAC pore classification.

185 3.2 Non-thermal plasma system characterization

186 The non-thermal plasma system was characterized by measuring the pulsed high voltage obtained
187 from the ignition coil. The waveform of the high voltage and corona current, from the ignition coil to
188 the remediation system, were measured by using a high voltage probe (Tektronix P6015A) and a
189 current probe (Tektronix A6021), respectively. A digital storage oscilloscope (Tektronix TDS2014)
190 was also used to display the waveforms. As shown in Fig. 4, a pulsed high voltage of 15 kV was
191 measured with the frequency of 100 Hz, approximately period time of 10 ms, rise time equal 70.46
192 μs , positive width 8.62 ms, and negative width 1.376 ms. This 15 kV was sufficient to generate a
193 considerable number of diverse radicals and active species (El-Tayeb et al. EEEIC 2015, El-Tayeb et
194 al. EEEIC 2016). These species are the hydroxyl radical (OH^*) and hydrogen atoms (H) from water
195 molecules. Also, humid air exposure to plasma generates ozone (O_3), singlet oxygen (O), hydrogen
196 peroxide (H_2O_2), and hydroperoxyl radical (HO_2) (Wang et al. 2008, Grabowski et al. 2006).



197 Fig. 4 Signal used in Corona Discharge Plasma
198

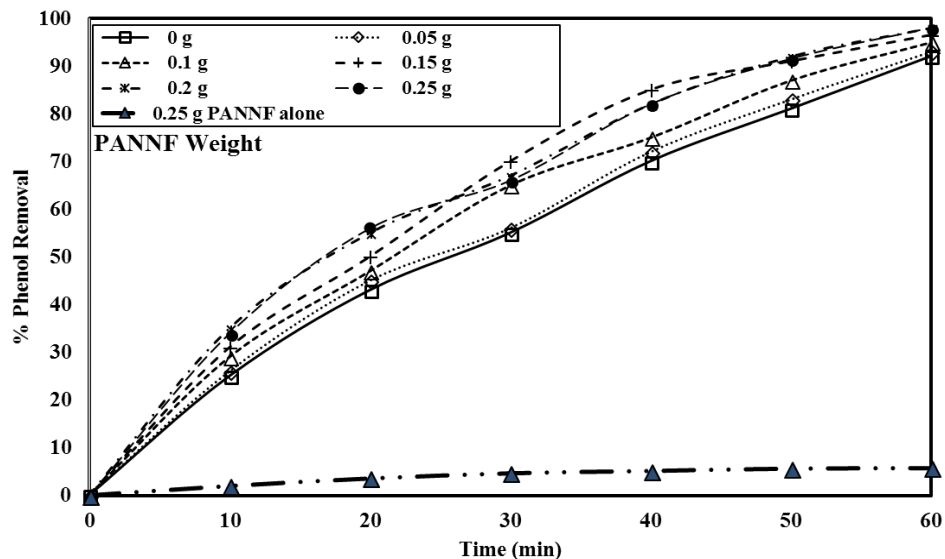
199 3.3 System performance for phenol remediation

200
 201 Regarding the investigation of PANNFs addition to the plasma system on the phenol removal process,
 202 different weights of PANNFs were mixed with 400 mL of various concentrations of phenol/water
 203 solutions. The remediation process time was kept at 60 min for all mixtures. Moreover, the energy
 204 consumed per unit volume, EE/O, and the energy yield for decolorization of phenol were examined
 205 for each parameter.

206
 207
 208

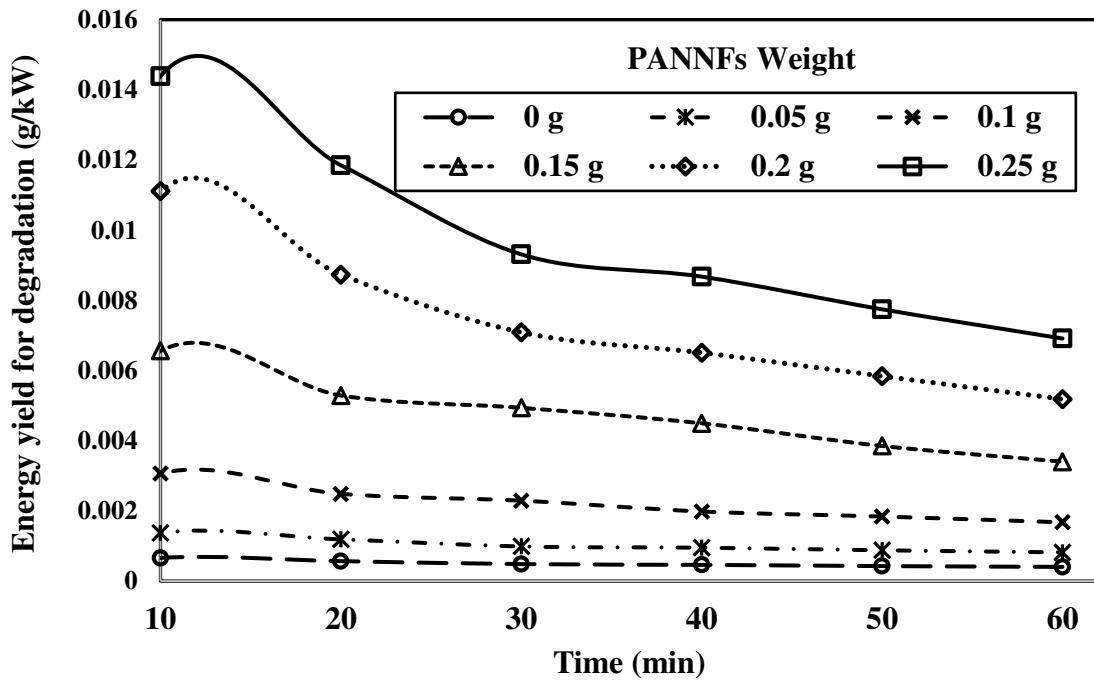
3.3.1 Effect of PANI addition

209 The effect of PANI presence was evaluated by fixing the initial concentration of phenol as 20 mg/L
 210 for all experiments at room temperature. Fig. 5 shows the phenol removal efficiency with time at
 211 different PANNFs weights. Generally, a rise in the phenol degradation efficiency was noticed with
 212 the increase of the PANNFs mass added. The results show that using plasma alone (0.0 mg/L
 213 PANNFs) removal of 92% of the initial phenol can be achieved within 60min, while at the same time,
 214 98% removal can be achieved using the dual system plasma and PANNFs of 250 mg/L. This may be
 215 referred to as the phenol adsorption onto the PANNFs surface. Furthermore, augmenting the amount
 216 of PANNF improved the active surface area, which was able to adsorb more phenol molecules. When
 217 0.25 g PANNFs was tested alone for the phenol removal (without plasma application), very low
 218 percentage removal was obtained. The maximum phenol removal was 5.7 % after one hour of
 219 treatment.

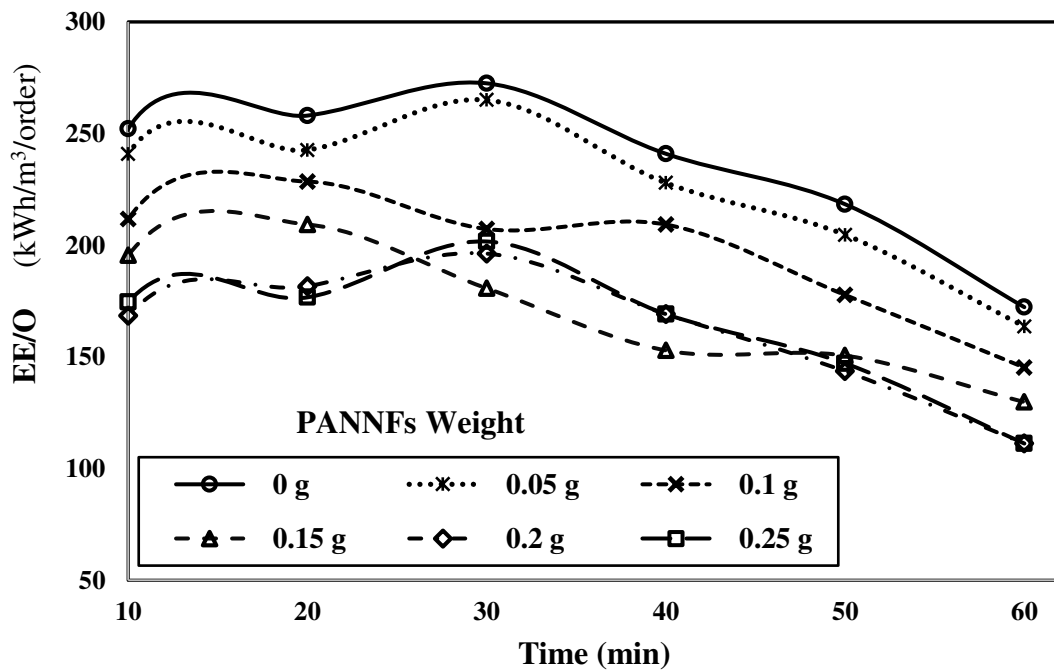


220
 221 Fig. 5 Phenol removal efficiency with different PANNF at initial phenol concentration of 20 mg/L.
 222
 223 The percentage removal of phenol using both removal techniques was always slightly more than the
 224 summation of the PANNFs and plasma alone systems. Accordingly, it could be concluded that there
 225 is a slight synergy effect between the two remediation systems. The plasma may affect the PANNFs
 226 surface by breaking the bond between the PANI chains and the chlorine atom, which may, in turn,
 227 increase the porosity or surface area of PANI.

228 Energy yield and EE/O for the phenol degradation process were shown in Fig. 6 and 7.



229 Fig. 6 The energy yield with different PANNF amounts at initial phenol concentration of 20 [mg/L].
230



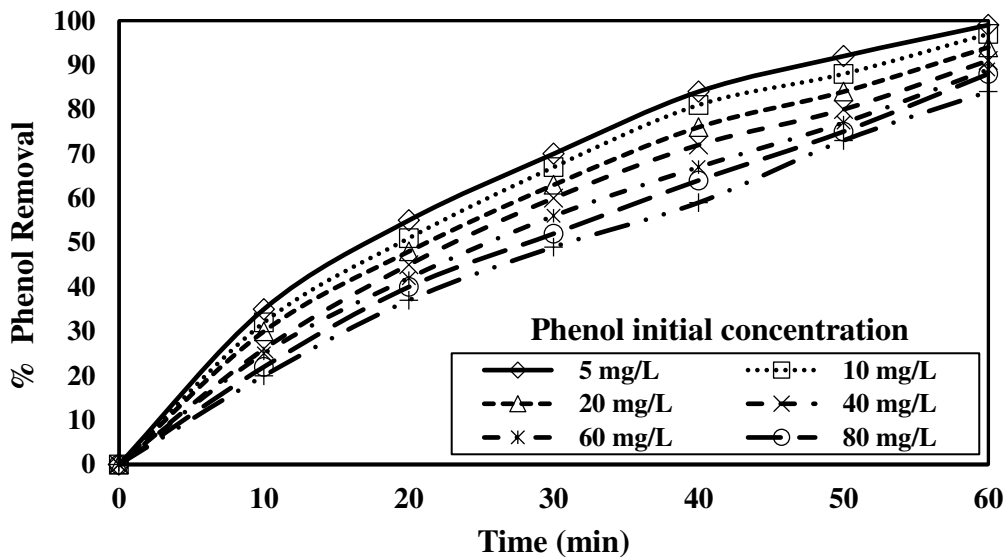
231 Fig. 7 EE/O with different PANNF amounts at initial phenol concentration of 20 mg/L.
232

233 It was observed that a better energy yield was attained with the increase of PANNFs addition. For
234 instance, after 60 min of treatment using the duel system (using 0.25 g of PANNFs), a dramatic
235 increase in the energy yield was noticed in comparison with the plasma alone system was acquired.
236 Generally, the energy yield changed proportionally with the percentage of decontamination D, as
237 described in Eqn. 4. The addition of PANNFs represents an active surface which adsorbed more
238 phenol. Moreover, plasma helps increase the PANNFs surface area by releasing the chlorine from the

239 polyaniline chains, which may help increase the phenol absorption. Based on Fig. 7, it was observed
240 that the EE/O decreased with the increase of PANNFs dosage. This may be because the system must
241 remove much more phenol when the initial concentration was high. Also, releasing chlorine ions
242 (widely used in water purification) may help purify the water.
243

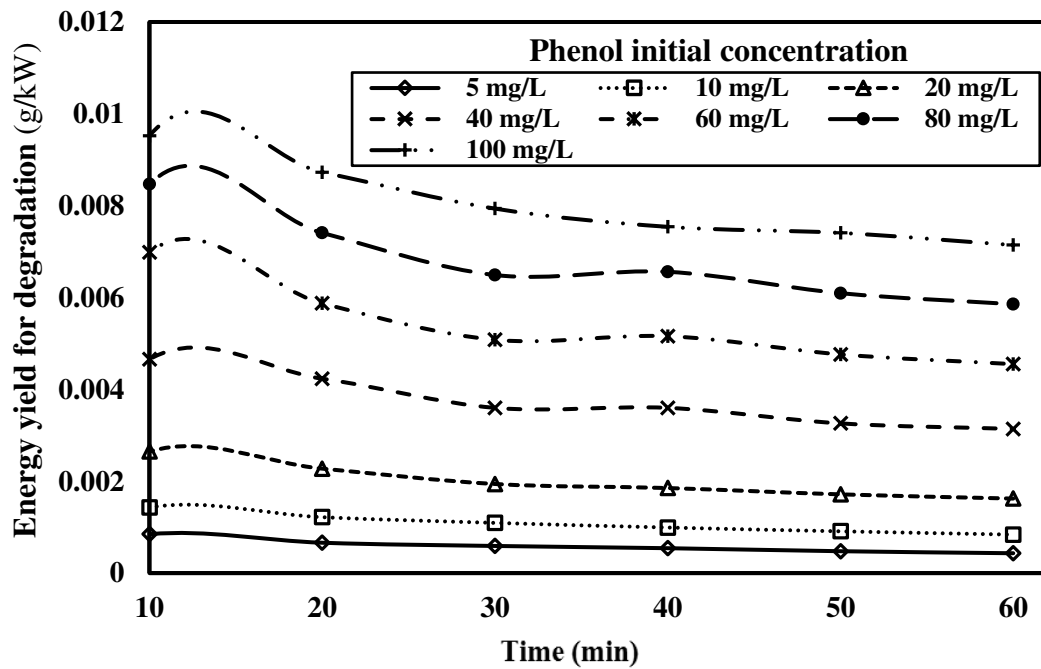
244 3.3.2 Effect of initial phenol concentration

245
246 To investigate the effect of the initial concentration of phenol on the overall degradation process, the
247 initial concentration of phenol was changed as (5, 10, 20, 40, 60, 80, and 100 mg/L) and a fixed
248 amount (0.2 g) of PANNFs was employed. Figure 8 shows the phenol removal efficiency with time
249 at different initial phenol concentrations. In general, a reduction in the phenol degradation efficiency
250 was noticed with the increase of the phenol concentration. The degradation efficiency was 99 % when
251 5 mg/L phenol concentration solution was used while it diminished to 84 % when 100 mg/L phenol
252 concentration was employed in a 60 min experiment. It seems to be reasonable for the dual
253 remediation system to reach this high efficiency in the case of low phenol concentration because of
254 the small amount of the phenol molecules. Besides, the system may need more time to reach the
255 mentioned high efficiency in case of high phenol concentration to get rid of all the contaminant
256 molecules.

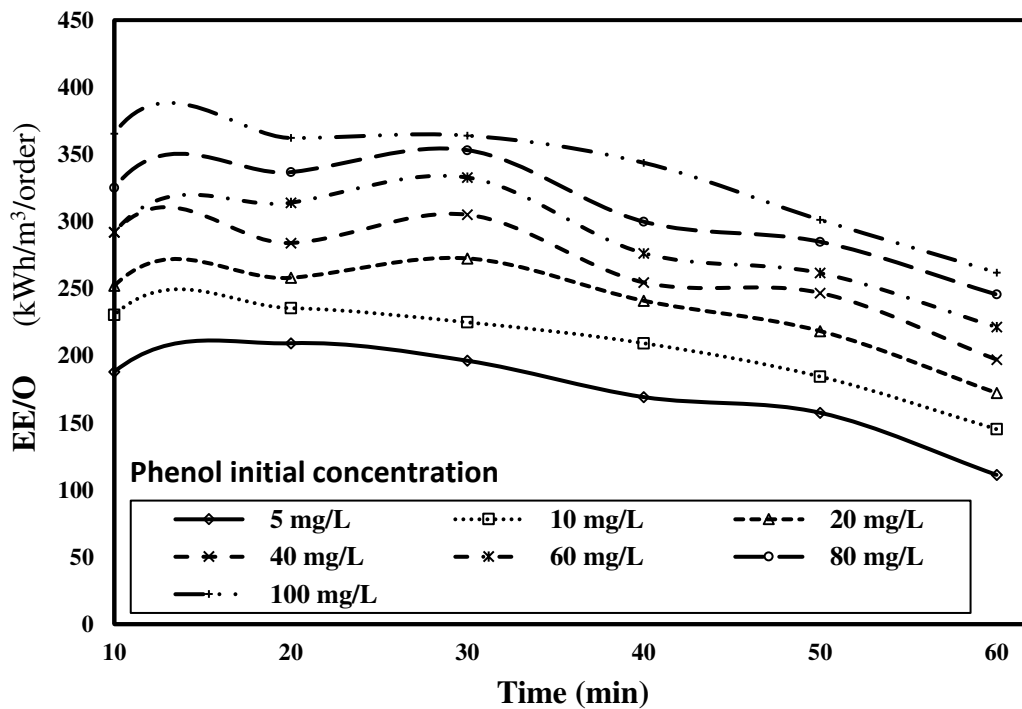


257
258 Fig. 8 Phenol removal efficiency with different phenol concentration 0.2 g of PANNF.
259
260 The energy yield for degradation was shown in Fig. 9. It was observed that higher energy yield
261 required with the higher phenol initial concentration. The used corona discharge plasma directly
262 degrades the phenol molecules. As it is known, phenol molecule includes a phenyl ring ($-C_6H_5$)
263 linked to a hydroxyl group ($-OH$), so the direct plasma treatment releases the hydroxyl group.
264 Accordingly, the more phenol concentration leads to more hydroxyl molecules released, i.e. more

265 radicals, which is desired for better phenol removal. In turn, the energy yield increases. Although, the
 266 higher phenol concentration, the lower phenol percentage removal obtained, the increase in the
 267 radicals is more than the reduction in the overall removal percentage.

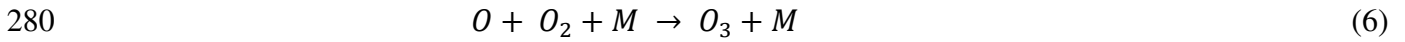
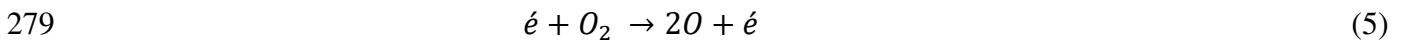


268 Fig. 9 Energy yield of degradation with different phenol initial concentrations at 0.2 g of PANNF.
 269
 270 Figure 10 showed the Electrical Energy per Order EE/O change with the time at different phenol
 271 initial concentrations. It was found that the EE/O increased with the enlargement of the initial phenol
 272 concentration. This is attributed to the increase in the concentration of OH radicals due to the phenol
 273 degradation when it exposed to the plasma.

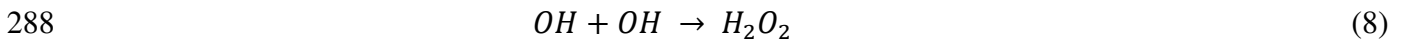
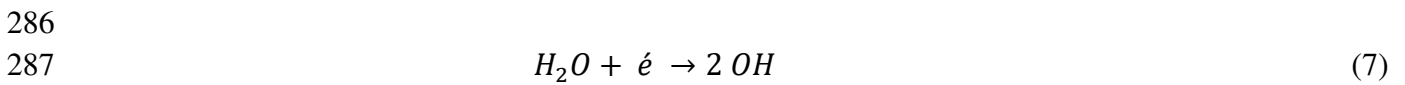


274 Fig. 10 EE/O with time at different phenol initial concentrations using 0.2 g of PANNF.
 275

276 Generally, ozone is generated in a two-steps process (Eqs. 5 and 6) when non-thermal plasma is
 277 applied to air, as a process gas, at atmospheric pressure and room temperature. These two steps are
 278 electrons utilization for O₂ molecules dissociation and described as follows (Wang et al. 2008):



281 Where *M* is a third collision partner involving: O, O₂, O₃, or N₂. Onto the liquid-plasma surface,
 282 another productive and desired reaction occurs due to plasma presence. This reaction generates OH
 283 radicals due to the exposor of gaseous water molecules and radical *O*, and it may follow the reaction
 284 in Eq. 7 (An 2011). Also, H₂O₂ may be generated due to the combination of OH radicals, as described
 285 in Eq. 8 (Wang et al. 2008).

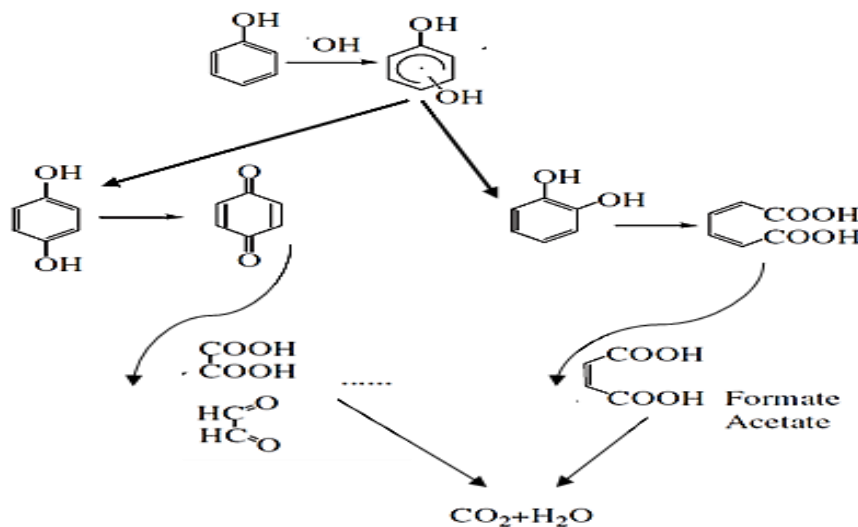


289
 290 The OH, H₂O₂, and O₃ radicals may be considered as the active primary radicals in the phenol
 291 degradation process (Grabowski et al. 2006, Iervolino et al. 2019).

292 3.3.3 Degradation mechanism

293 Phenol degradation using plasma may follow several mechanisms. One of the proposed mechanisms
 294 for the phenol degradation process is the formation of carbon dioxide and water passing some
 295 intermediate components. The hydroxyl group may play a vital role in this degradation process
 296 (Zhang 2013, Wang et al. 2008). Catechol and hydroquinone are the core primary by-products of
 297 phenol, which formed via ^{*}OH reaction with the aromatic ring at the ortho or para-positions.

298



299

300 Fig. 11 Schematic diagram for the proposed phenol degradation process mechanisms using the developed
 301 dual remediation system.

302 Furthermore, the redox reaction of hydroquinone produced 1,4-benzoquinone while the unstable
303 catechol transformed into 1,2-benzoquinone. A different mechanism was also proposed to describe
304 the degradation process using the $\cdot\text{OH}$ group. In this second case, aliphatic by-products (formic acid,
305 oxalic acid, and aldehydes, etc.) were produced by the continuous oxidation of the aromatic rings. All
306 the produced by-products were mineralized into carbon dioxide and water at the end of reactions.
307 These two mechanisms are illustrated in Fig. 11.

308

309 **4 Conclusion**

310 A dual remediation system utilizes two different removal techniques for phenol degradation; non-
311 thermal plasma accompanied by adsorption of phenol onto the surface of polyaniline nanofiber
312 PANNFs was designed. Upon the results, the prepared polyaniline showed a nanofibrous structure
313 with fibers of an average diameter of 40 nm and a surface area of 26.42 m²/g. The phenol degradation
314 efficiency of 92 % was obtained in 60 min when plasma treatment was used alone, while 98 % phenol
315 was removed when 0.25 g of PANNFs was employed (20 mg/L initial phenol concentration).
316 Furthermore, the dual remediation system lowered the consumed energy by 30 % (according to the
317 EE/O calculations). Generally, a slight synergistic effect between the non-thermal plasma oxidation
318 and PANI adsorption techniques was recorded. PANI surface captured the phenol molecules and may
319 make it easy for plasma to degrade the collected phenol molecules instead of scattered molecules.

320 **Ethical Approval**

321 Not applicable

322 **Consent to Participate**

323 Not applicable

324 **Consent to Publish**

325 Not applicable

326 **Authors Contributions**

327 Dr. Ahmed EL-Tayeb: First and soul author of the paper in part of corona discharge plasma work,
328 drafted the paper and revised the manuscript.

329 Dr. Hussain Noby: Edited and contributed in some section in write up. In addition, contributed in part
330 of polyaniline nanofiber PANNFs work

331 Prof. Ahmed Hassan EL-Shazly: Project leader and edited and contributed sections of the manuscript.

332 Prof. Marwa Elkady: Assist in Project, edited and contributed sections of the manuscript.

333 **Funding**

334 Not applicable

335 **Competing Interests**

336 The authors declare that they have no competing interests.

337 **Availability of data and materials**

338 All data generated or analyzed during this study are included in this published article.

339 **References:**

- 340 A. El-Tayeb, A. H. El-Shazly and M. F. Elkady, “Impacts of Different Salts on the Degradation of
341 Acid Blue 25 Dye Using Non-Thermal Plasma”, The 16th IEEE International Conference on
342 Environment and Electrical Engineering (EEEIC 2016), Florence, Italy, 7-10 June, (2016).
- 343 A. El-Tayeb, A. H. El-Shazly and M. F. Elkady, “Investigation the Influence of Different Salts on the
344 Degradation of Organic Dyes Using Non-Thermal Plasma,” *Energies* 2016, 9(11), 874;
345 DOI:10.3390/en9110874.
- 346 A. El-Tayeb, A. H. El-Shazly, M. F. Elkady, and A. Abdel-Rahman, “Simulation and Experimental
347 Study for Degradation of Organic Dyes Using Dual pin-to-plate Corona Discharge Plasma
348 reactors for Industrial Wastewater Treatment,” *Contrib. Plasma Phys.*, 56, 855–869, DOI:
349 10.1002/ctpp.201500080, (2016).
- 350 A. El-Tayeb, A.H. El-Shazly, M.F Elkady, A. Abdel-Rahman, “Non-thermal plasma as a new
351 advanced technique for intensifying the industrial wastewater treatment,” *Desalination and
352 Water Treatment* 61 (2017) 230–239 DOI: 10.5004/dwt.2016.11343.
- 353 A. El-Tayeb, A.H. El-Shazly, M.F. Elkady, and A. Abdel-Rahman, “Decolorization of Acid Blue 25
354 Dye by Non-Thermal Plasma Advanced Oxidation Process for Industrial Wastewater Treatment”,
355 The 15th IEEE International Conference on Environment and Electrical Engineering (EEEIC
356 2015), Rome, Italy, June 10-13, 2015.
- 357 A. El-Tayeb, A.H. El-Shazly, M.F. Elkady, and A. Abdel-Rahman, “Investigation of the
358 Decolorization Efficiency of Two Pin-to-Plate Corona Discharge Plasma System for Industrial
359 Wastewater Treatment,” *Plasma Phys. Rep.* 42: 887-899. DOI: 10.1134/S1063780X16090026,
360 (2016).
- 361 A., S. Rather, A. El-Shazly, Sh. F. Zaman, M. A. Daous, A. A. Al-Zahrani, Preparation of activated
362 carbon from fly ash and its application for CO₂ capture, *Korean J. Chem. Eng.*, 32(4), (2015).
- 363 B. Jiang, J. Zheng, Sh. Qiu, M. Wu, Q. Zhang, Z. Yan, Q. Xue, Review on electrical discharge plasma
364 technology for wastewater remediation, *Chemical Engineering Journal*, 236, 348–368 (2014).
- 365 B. Jiang, J. Zheng, X. Lu, Q. Liu, M. Wu, Z. Yan, Sh. Qiu, Q. Xue, Z. Wei, H. Xiao, M. Liu,
366 Degradation of organic dye by pulsed discharge non-thermal plasma technology assisted with
367 modified activated carbon fibers, *Chemical Engineering Journal* 215–216, 969–978 (2013).
- 368 C. Xu, H. Chen, and F. Jiang, “Adsorption of perflourooctane sulfonate (PFOS) and
369 perfluorooctanoate (PFOA) on polyaniline nanotubes,” *Colloids Surfaces A Physicochem. Eng.*
370 *Asp.*, vol. 479, pp. 60–67, 2015.
- 371 F. Belaib, A. Meniai, M. Lehocine, Elimination of Phenol by Adsorption onto Mineral / Polyaniline
372 Composite Solid Support Mineral / Polyaniline Composite Solid, *Energy Procedia* 18, 1254 –
373 1260 (2012).
- 374 F. J. Bosi, F. Tampieri, E. Marotta, R. Bertani, D. Pavarin, C. Paradisi, Characterization and
375 comparative evaluation of two atmospheric plasma sources for water treatment, *Plasma Process
376 and Polymers*;15:e1700130, <https://doi.org/10.1002/ppap.201700130>, (2018).
- 377 G. An, Y. Sun, T. Zhu, X. Yan, "Degradation of phenol in mists by a non-thermal plasma reactor,"
378 *Chemosphere* 84, 1296–1300, (2011).

- 379 G. Iervolino, V. Vaiano, V. Palma, "Enhanced removal of water pollutants by dielectric barrier
380 discharge nonthermal plasma reactor," *Separation and Purification Technology* 215, 155–162,
381 (2019).
- 382 G. Ni, G. Zhao, Y. Jiang, J. Li, Y. Meng, X. Wang, Steam Plasma Jet Treatment of Phenol in Aqueous
383 Solution at Atmospheric Pressure. *Plasma Processes and Polymers*, 10: 353-363.
384 doi:10.1002/ppap.201200155, (2013).
- 385 H. Noby, A.H. El-Shazly, M.F. Elkady, M. Ohshima, Adsorption Profiles of Acid Dye using
386 Synthesized Polyaniline Nanostructure with Different Morphologies, *Chemical Engineering*
387 *Journal of Japan*, 50(3):170-177 (2017).
- 388 H. Noby, A.H. El-Shazly, M.F. Elkady, M. Ohshima, Investigation of the Parameters affecting CO₂-
389 assisted Polyaniline Polymerization, *MATEC Web of Conferences*, 69, 04001 (2016).
- 390 H. Noby, A.H. El-Shazly, M.F. Elkady, M. Ohshima, Novel preparation of Self-assembled HCl-
391 doped Polyaniline Nanotubes using compressed CO₂-assisted Polymerization, *Polymer* 156,
392 (2018), 71–75.
- 393 H. Noby, A.H. El-Shazly, M.F. Elkady, M. Ohshima, Strong Acid Doping for the Preparation of
394 Conductive Polyaniline Nanoflowers, Nanotubes, and Nanofibers, *Polymer*, 182, (2019), 121848.
- 395 H. Seo, S. Ameen, M. Akhtar, M. Shin, Structural, morphological, and sensing properties of layered
396 polyaniline nanosheets towards hazardous phenol chemical, *Talanta* 104, 219-227, (2013).
- 397 H. Wang, J. Li, X. Quan, Y. Wu, Enhanced generation of oxidative species and phenol degradation
398 in a discharge plasma system coupled with TiO₂ photocatalysis, *Applied Catalysis B:*
399 *Environmental* 83, 72–77, (2008).
- 400 J. Wang, K. Zhang, L. Zhao, Sono-assisted synthesis of nanostructured polyaniline for adsorption of
401 aqueous Cr(VI): Effect of protonic acids, *Chemical Engineering Journal* 239 (2014) 123–131.
- 402 K. Kaneko, Determination of pore size and pore size distribution. 1. Adsorbents and catalysts, *J.*
403 *Membrane Sci.* 96, 59-89 (1994).
- 404 L. Ai, J. Jiang, R. Zhang, Uniform polyaniline microspheres: A novel adsorbent for dye removal from
405 aqueous solution, *Synthetic Metals* 160 (2010) 762–767.
- 406 L. R. Grabowski, E. M. van Veldhuizen, A. J. M. Pemen, W. R. Rutgers, Corona above water reactor
407 for the systematic study of aqueous phenol degradation, *Plasma Chemistry, and Plasma*
408 *Processing*, Vol. 26, No. 1, (2006).
- 409 M. Ayad, G. El-Hefnawy, S. Zaghlol, Facile synthesis of Polyaniline nanoparticles; its adsorption
410 behavior, *Chemical Engineering Journal* 217 (2013) 460–465.
- 411 P. Lukes and B. R. Locke, Degradation of Substituted Phenols in a Hybrid Gas–Liquid Electrical
412 Discharge Reactor, *Industrial & Engineering Chemistry Research* 44, 2921, (2005).
- 413 P. Sunka, Pulse electrical discharges in water and their applications, *Physics of Plasmas* 8, 2587
414 (2001).
- 415 S. Kulkarni, R. Tapre, S. Patil, M. Sawarkar, Adsorption of Phenol from Wastewater in Fluidized
416 Bed Using Coconut Shell Activated Carbon, *Procedia Engineering* 51, 300 – 307 (2013).
- 417 X. Hao, X. Zhang, L. Lei, Degradation characteristics of toxic contaminant with modified activated
418 carbons in an aqueous pulsed discharge plasma process, *CARBON* 47, 153 – 161 (2009).
- 419 Y. Hayashi, E. Wahyudiono, S. Macmudah, N. Takada, H. Kanda, K. Sasaki, and M. Goto,
420 Decomposition of methyl orange using pulsed discharge plasma at atmospheric pressure: effect
421 of the different electrode, *Jpn. J. Appl. Phys.* 53 1-8, (2014).
- 422 Y. Zhang, Q. Xin, Y. Cong, Q. Wang, B. Jiang, Application of TiO₂ nanotubes with pulsed plasma
423 for phenol degradation, *Chemical Engineering Journal* 215–216, 261–268 (2013).

Figures

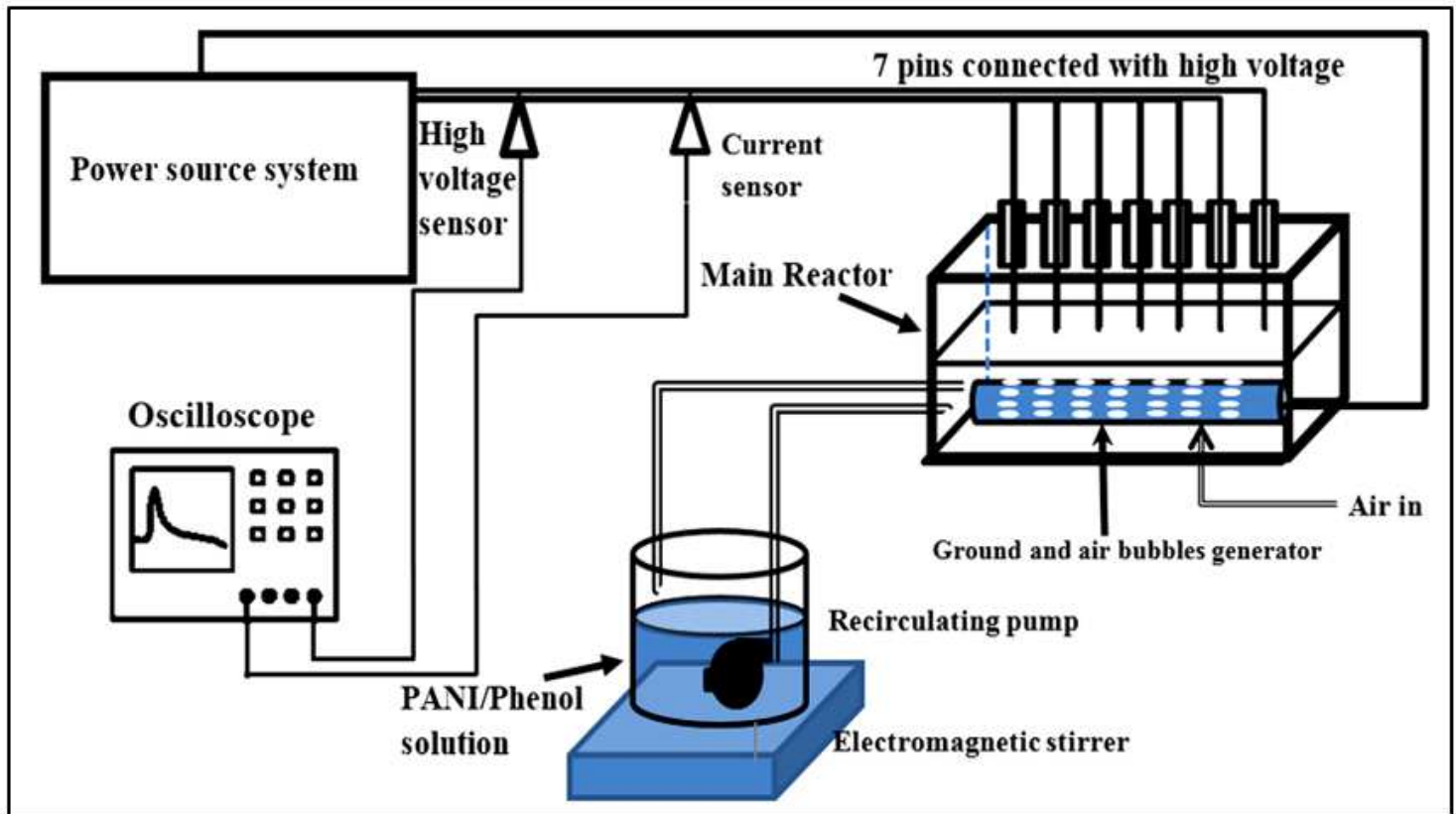


Figure 1

Schematic diagram of the designed new remediation system used for phenol removal.

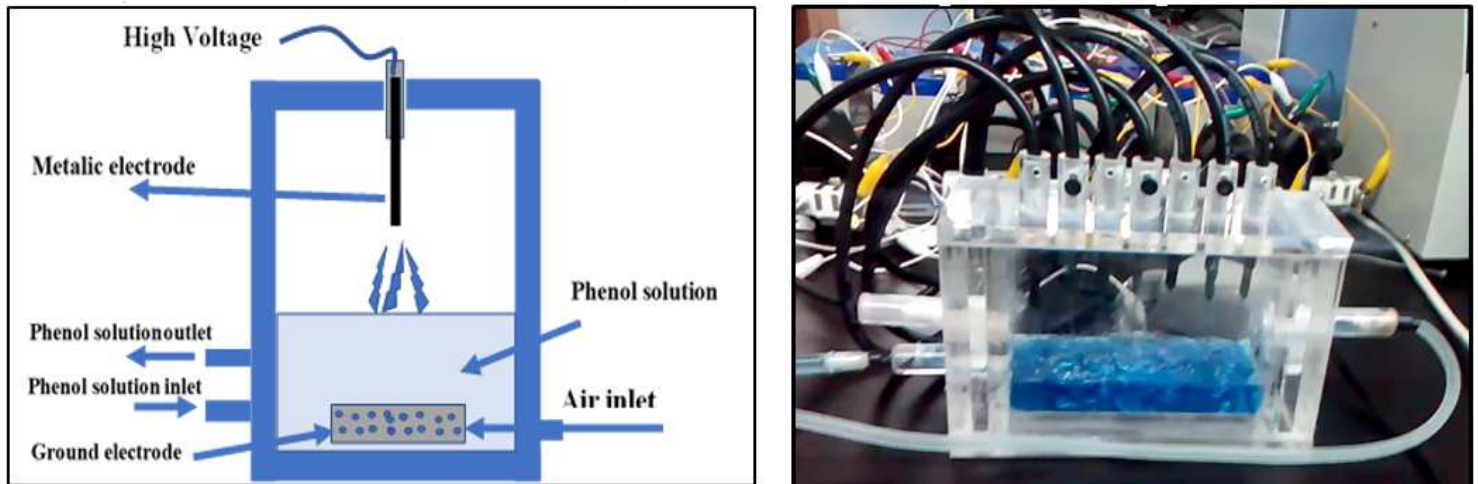


Figure 2

Schematic diagram of the main reactor's side view.

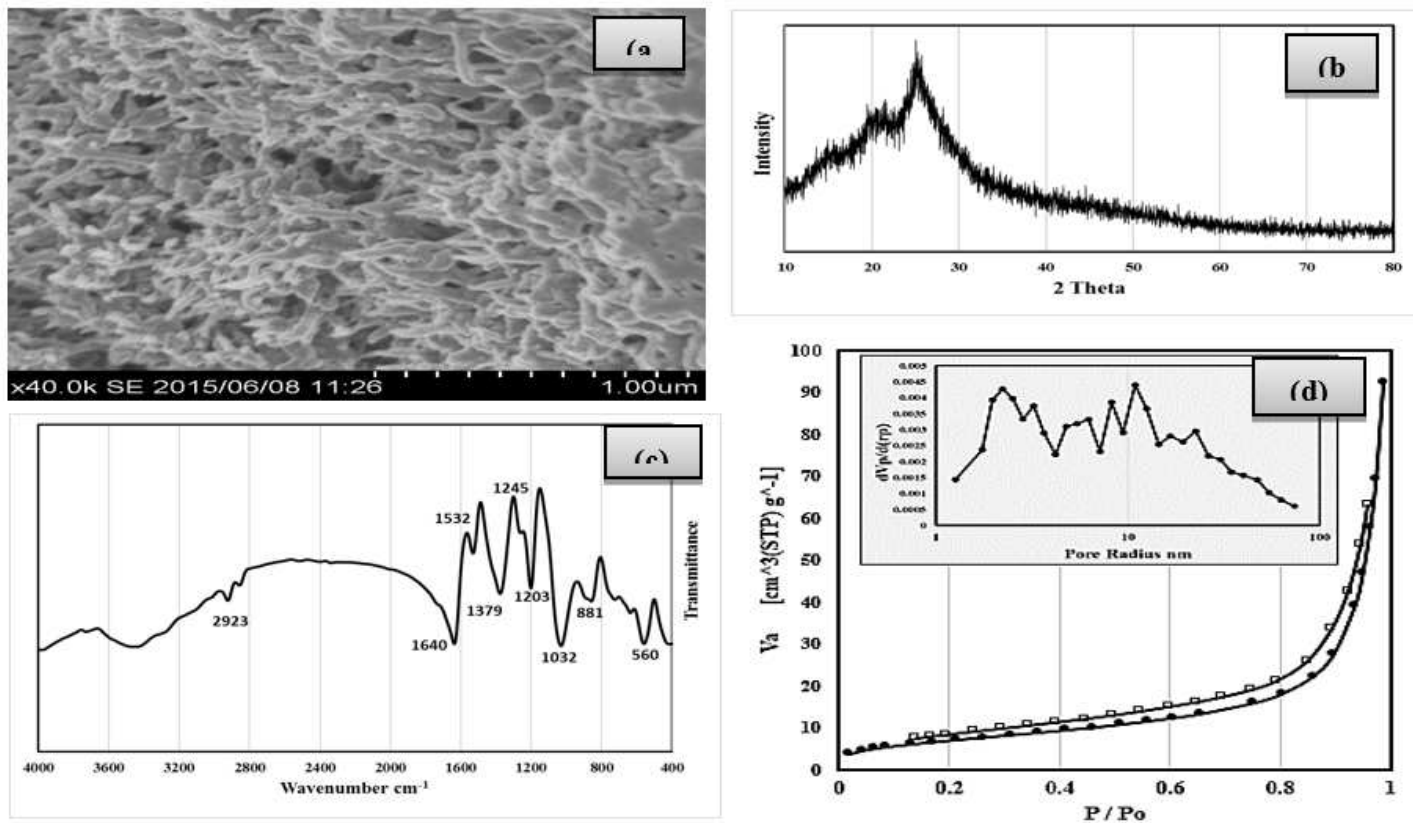


Figure 3

(a) SEM image, (b) XRD, (c) FT-IR, and (d) N_2 adsorption/desorption isotherm and pore size distribution for the produced PANI.

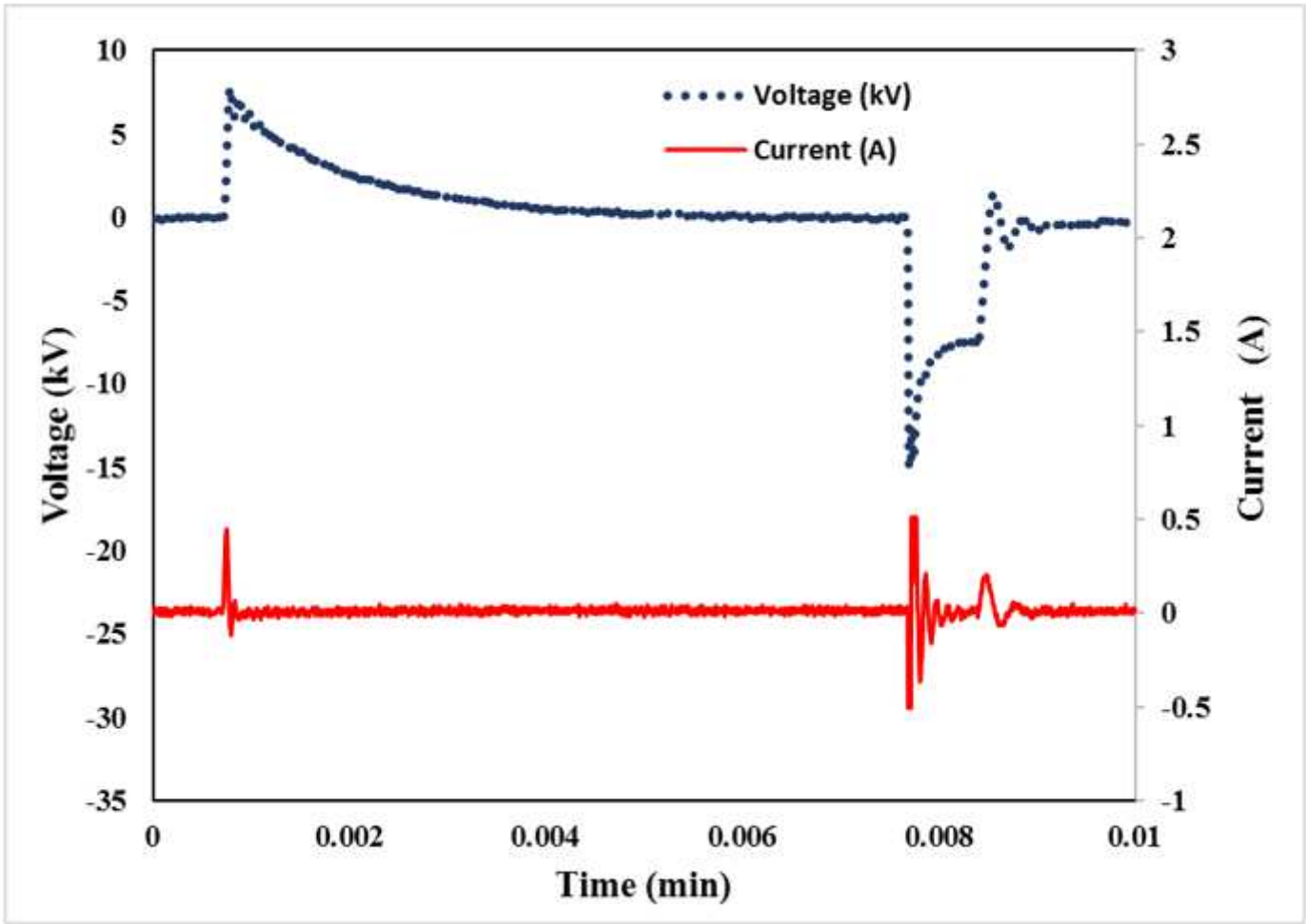


Figure 4

Signal used in Corona Discharge Plasma

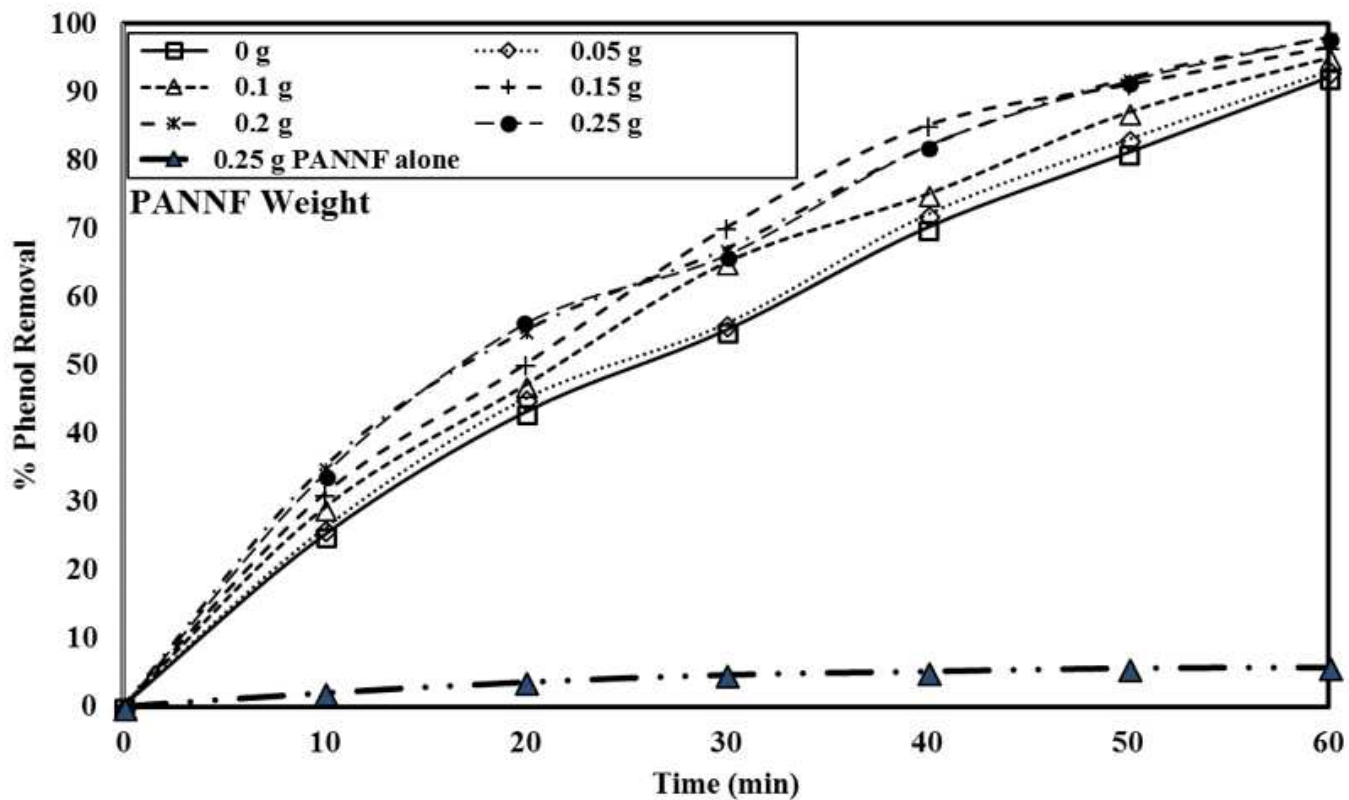


Figure 5

Phenol removal efficiency with different PANNF at initial phenol concentration of 20 mg/L.

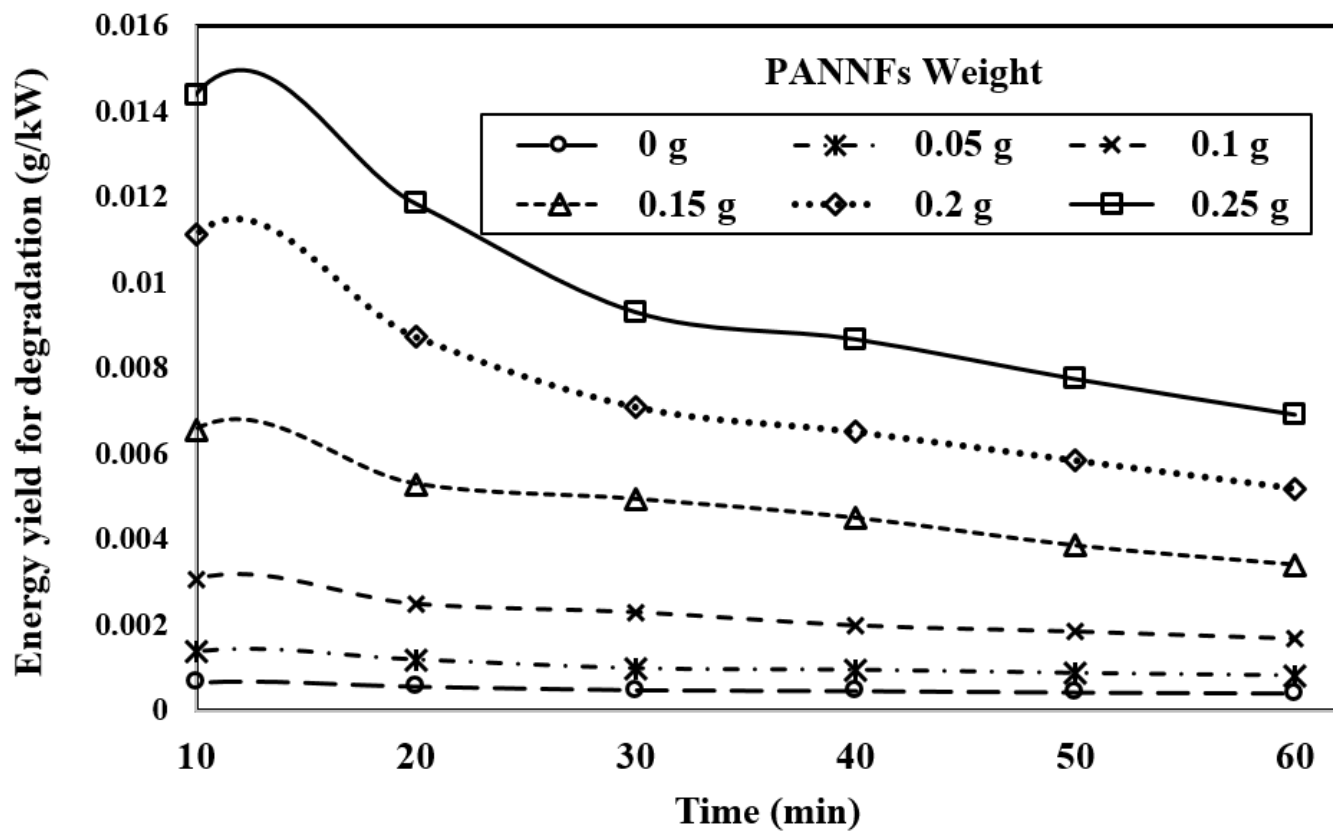


Figure 6

The energy yield with different PANNF amounts at initial phenol concentration of 20 [mg/L].

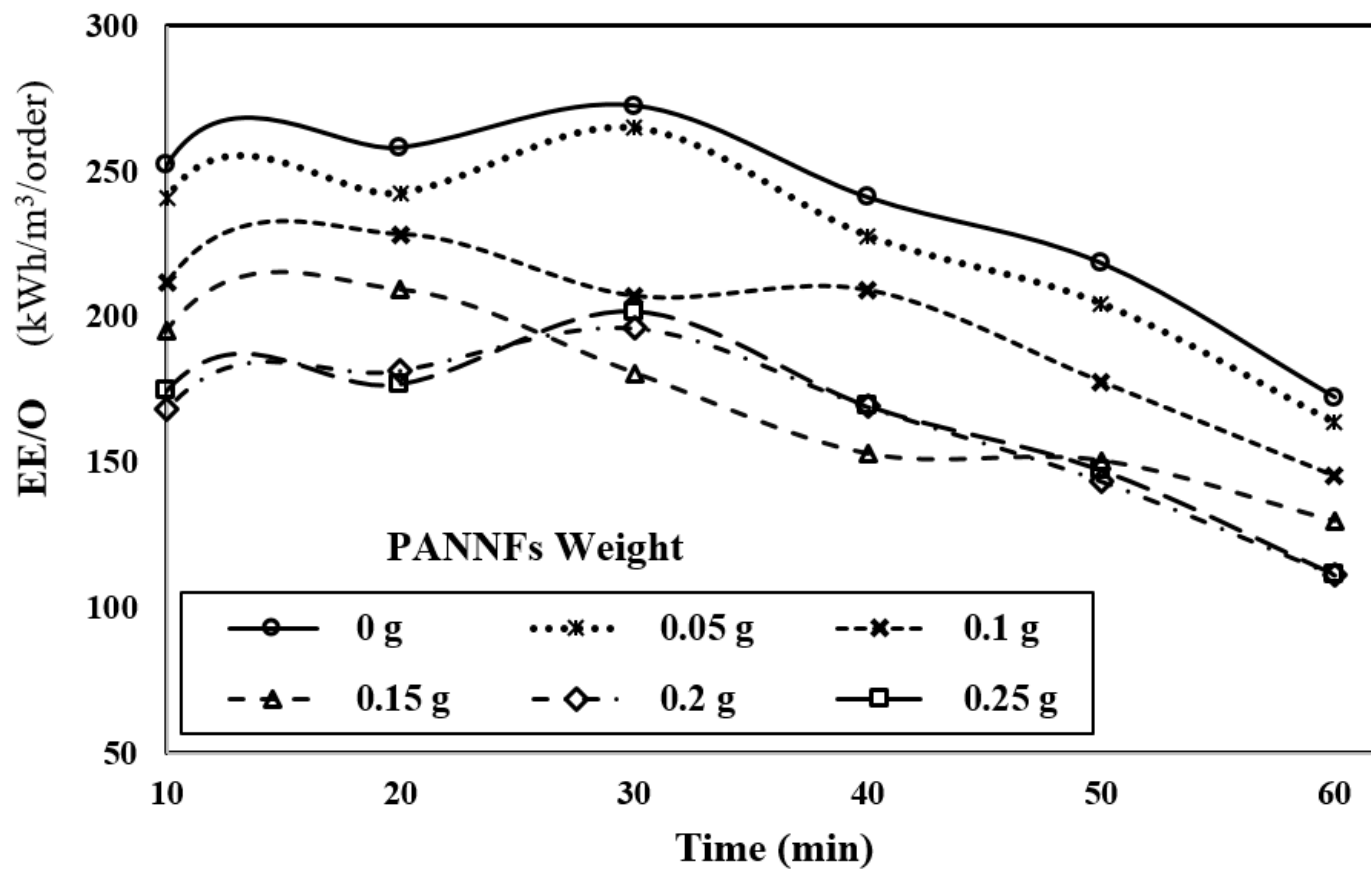


Figure 7

EE/O with different PANNF amounts at initial phenol concentration of 20 mg/L.

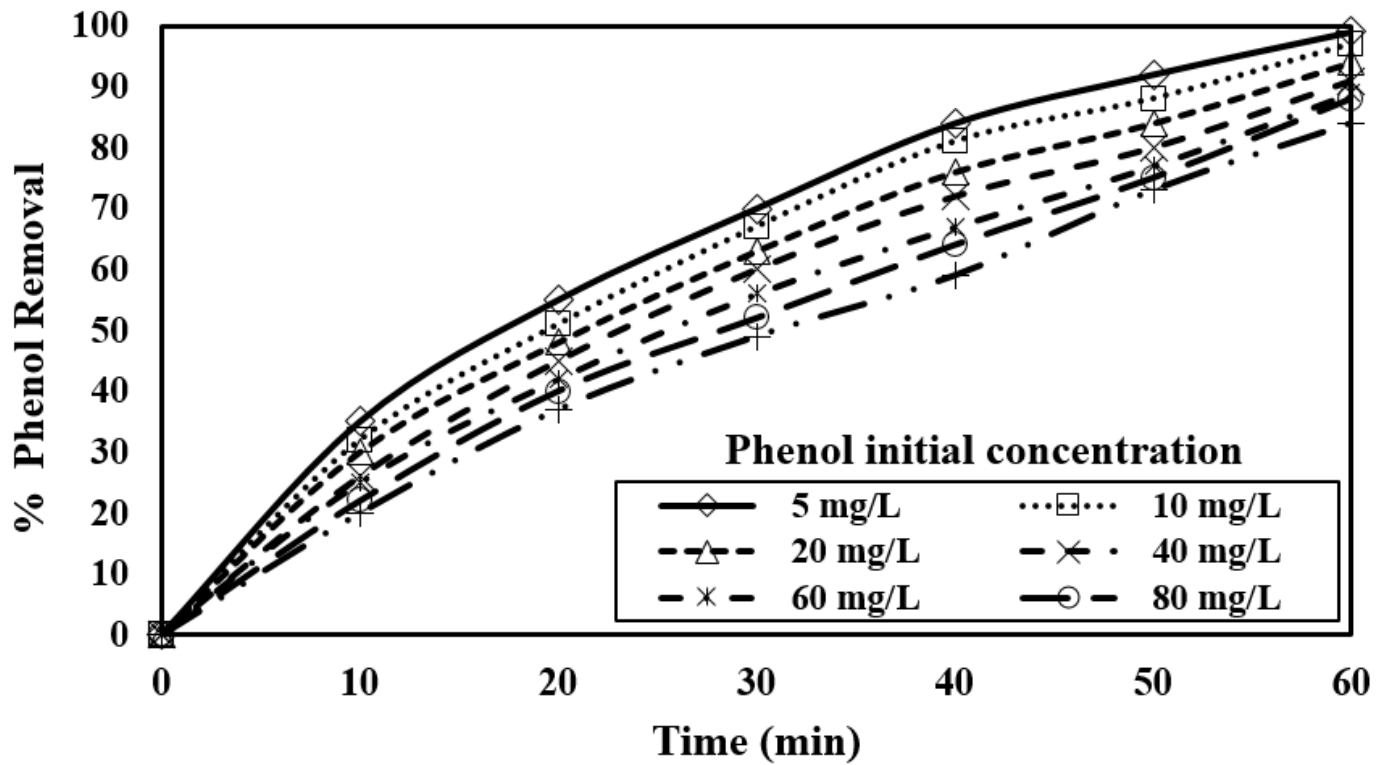


Figure 8

Phenol removal efficiency with different phenol concentration 0.2 g of PANNF.

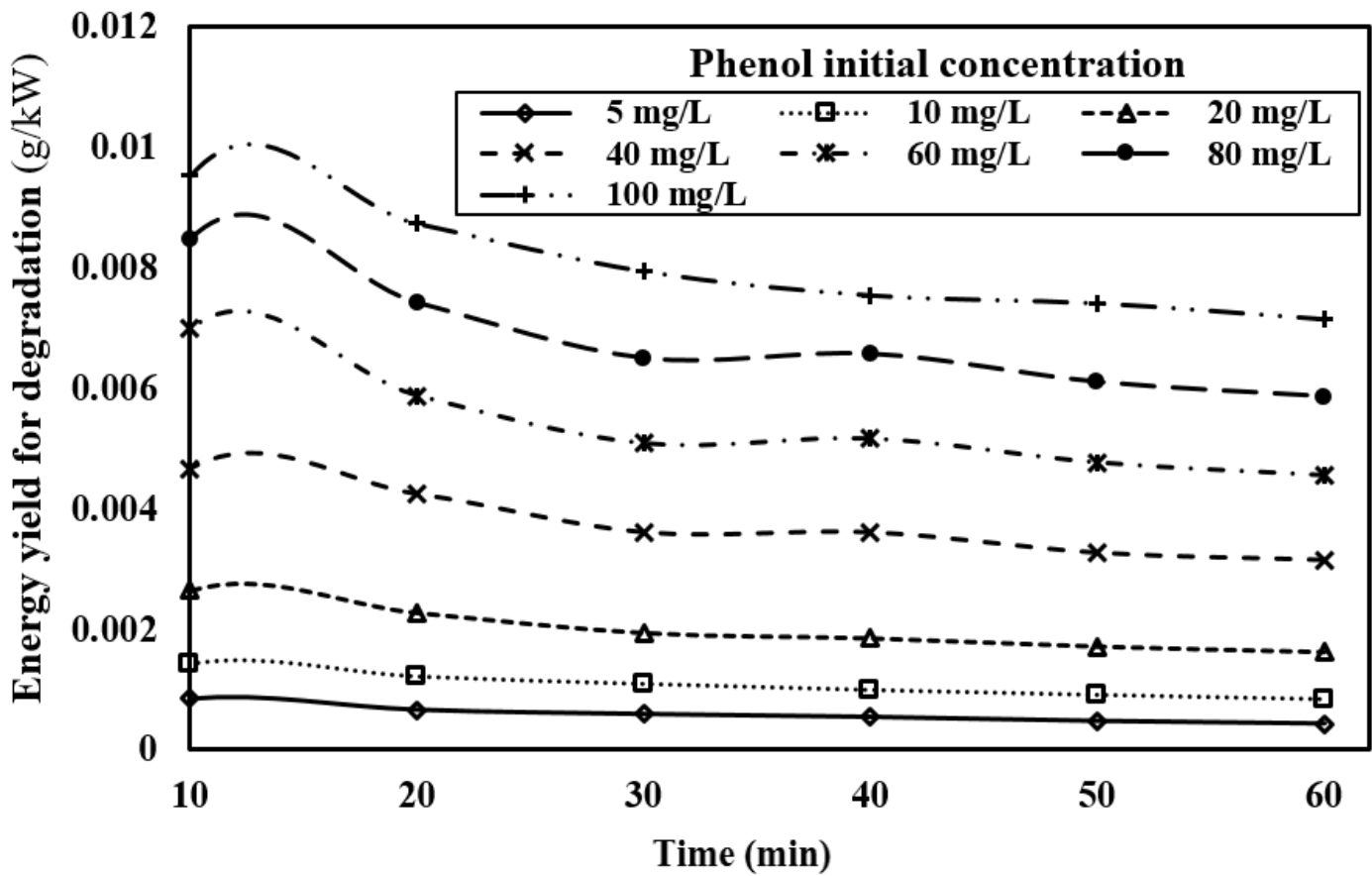


Figure 9

Energy yield of degradation with different phenol initial concentrations at 0.2 g of PANNF.

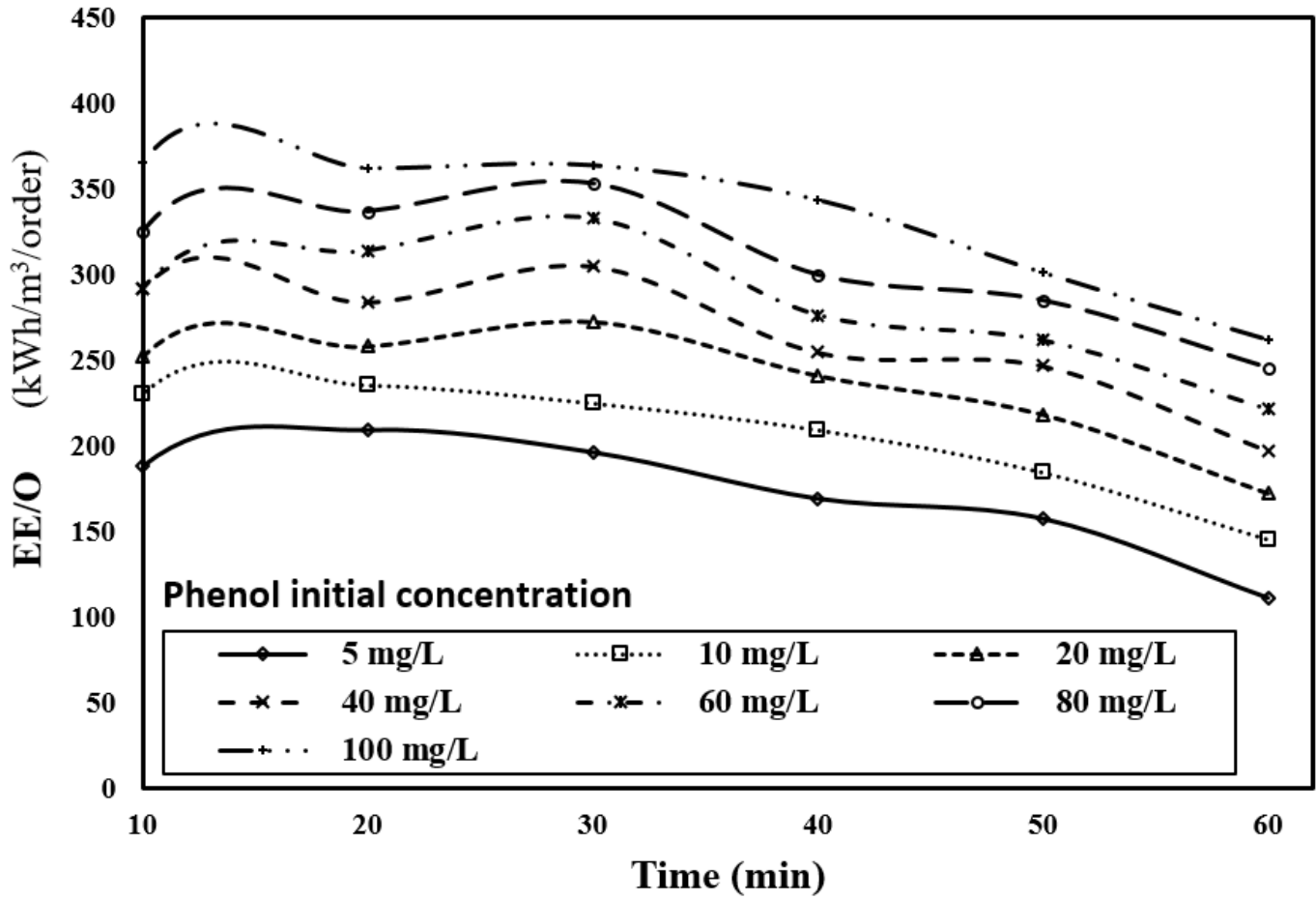


Figure 10

EE/O with time at different phenol initial concentrations using 0.2 g of PANNF.

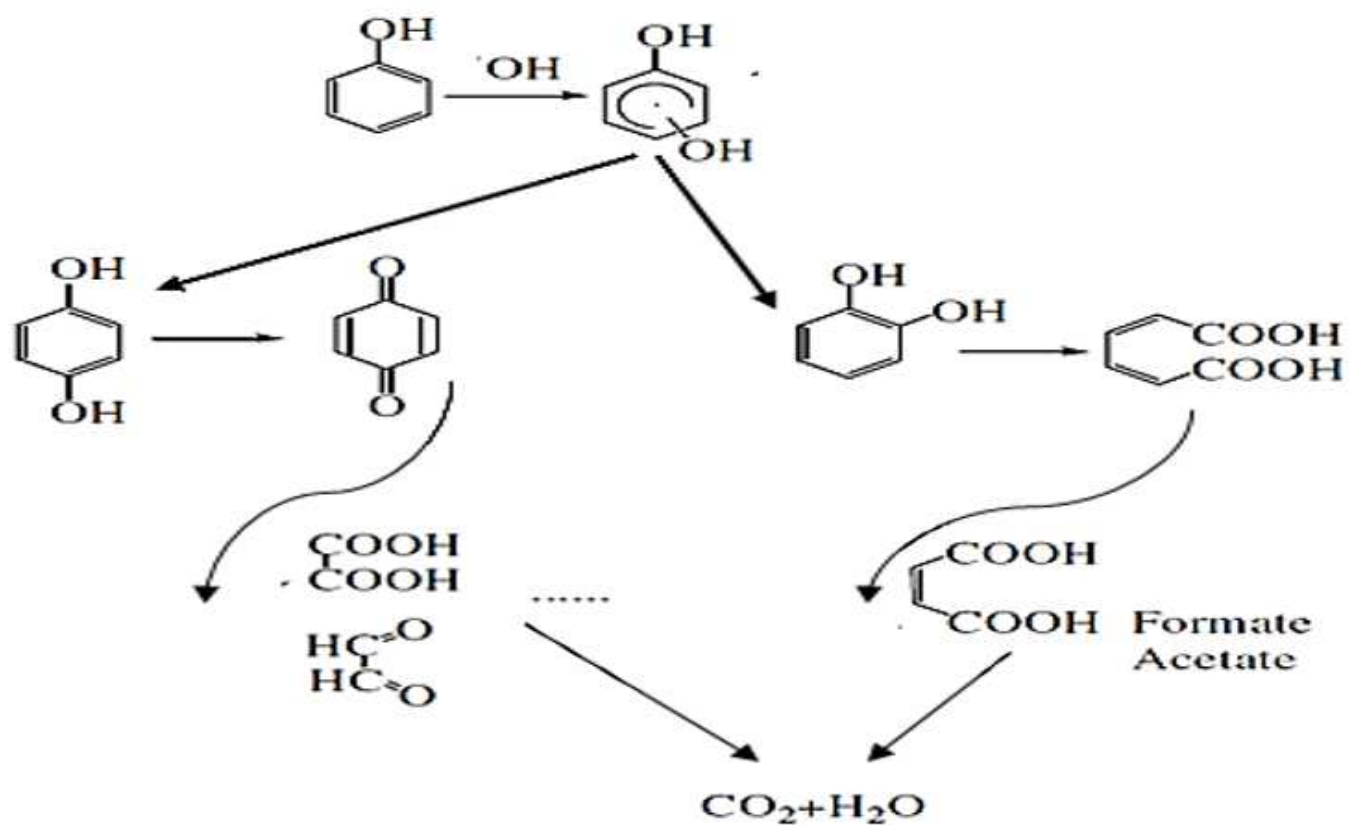


Figure 11

Schematic diagram for the proposed phenol degradation process mechanisms using the developed dual remediation system.

Supplementary Files

This is a list of supplementary files associated with this preprint. Click to download.

- [GraphicalAbstarct.png](#)